TIDALLY DRIVEN EXCHANGE IN AN ARCHIPELAGO STRAIT

BIOLOGICAL AND OPTICAL RESPONSES

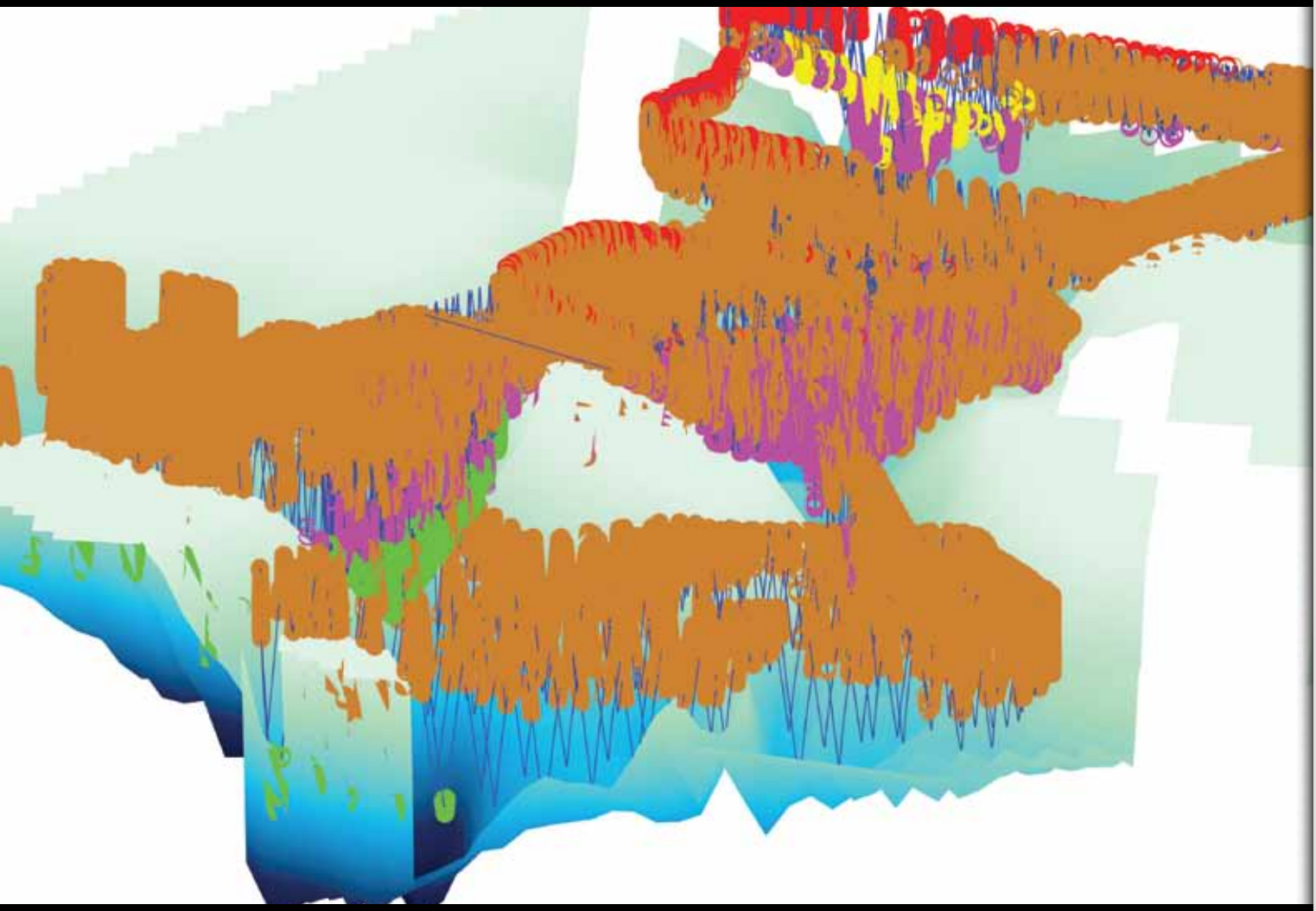

BY BURTON H. JONES, CRAIG M. LEE, GERARDO TORO-FARMER, EMMANUEL S. BOSS, MICHAEL C. GREGG, AND CESAR L. VILLANOY

ABSTRACT. Measurements in San Bernardino Strait, one of two major connections between the Pacific Ocean and the interior waters of the Philippine Archipelago, captured 2–3 m s^{-1} tidal currents that drove vertical mixing and net landward transport. A TRIAXUS towed profiling vehicle equipped with physical and optical sensors was used to repeatedly map subregions within the strait, employing survey patterns designed to resolve tidal variability of physical and optical properties. Strong flow over the sill between Luzon and Capul islands resulted in upward transport and mixing of deeper high-salinity, low-oxygen, high-particle-and-nutrient-concentration water into the upper water column, landward of the sill. During the high-velocity ebb flow, topography influences the vertical distribution of water, but without the diapycnal mixing observed during flood tide. The surveys captured a net landward flux of water through the narrowest part of the strait. The tidally varying velocities contribute to strong vertical transport and diapycnal mixing of the deeper water into the upper layer, contributing to the observed higher phytoplankton biomass within the interior of the strait.

INTRODUCTION

Strong archipelago throughflow, such as that observed in the Philippines, interacts with complex bathymetry to produce a range of energetic flow regimes. Orographic steering by island topography can influence the wind and thermal forcing of the region, introducing small-scale lateral variations in the forcing fields (Pullen et al., 2008). Subsurface topography, at least as complex as the terrestrial topography, includes many between-island straits and sills with complex shapes. Historically, the interior seas of the archipelago have been relatively underexplored, with few in situ, subsurface observations. Remotely sensed ocean color provides some indication of the probable distributions of phytoplankton and particles as well as related properties in the region (e.g., Figure 1). However, in the absence of appropriate ground truth measurements, the possible confounding optical influences of the coastal region (e.g., adjacency effects, bottom contributions) produce significant uncertainty in ocean color products. In addition, remotely sensed ocean color is limited to the upper few meters of the water column, limiting its utility for studying the complex subsurface processes that can affect optical variability.

This study examines flow dynamics and the resulting distribution of biogeochemical and bio-optical parameters in the San Bernardino Strait region (Figure 1, white box) surveyed during the 2009 PhilEx Intensive Observational Period (IOP-09). To our knowledge, few previous data exist from this region; even the mean net transport is uncertain (Gordon et al., 2011). The earliest modern observations were collected by the US Coast and Geodetic Survey in the 1920s (http://www.photolib.noaa.gov/htmls/cgs00029.htm), but, to our knowledge, no data from this effort have been published. The Japanese fleet passed through the strait on its way to a surprise attack on the American fleet during the World War II Battle of Leyte Gulf, providing historical significance to the region. Recently, the strait's strong tidal currents have made it an area of interest for tidal power generation (Jones and Rowley, 2002).

San Bernardino Strait is a relatively narrow passage on the northeastern side of the Philippine Archipelago. The strait is about 6.5-km wide at its narrowest point, between Luzon and Capul islands, where sill depth is about 90 m at the channel's center (Figure 2). Current speeds of up to nearly 4.5 m s^{-1} have been reported near the southern tip of Capul (Peña and Mariño, 2009), and, one of the authors has observed current speeds of roughly 4 m s^{-1} over the sill during prior efforts in the area.

Straits and their associated sills have been the subject of investigation for a long period in modern oceanography. Some of the earliest and most sustained interest has been in the Strait of Gibraltar

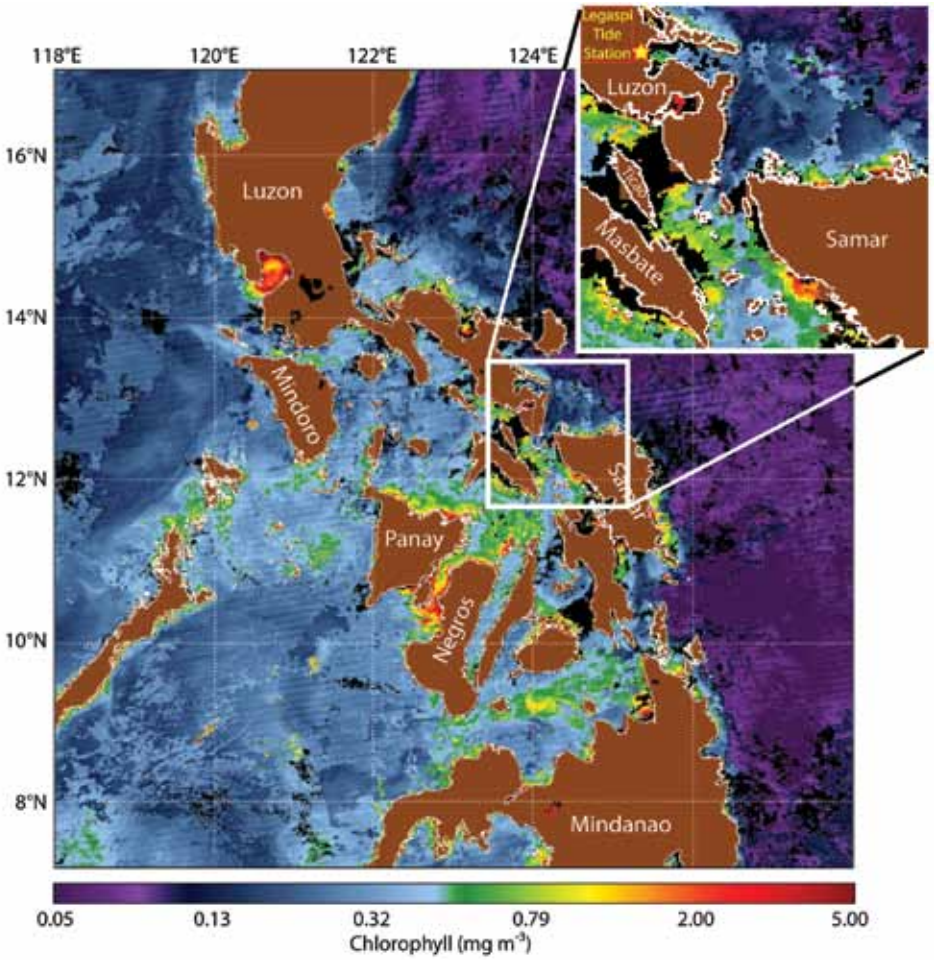

Figure 1. Ocean color image of chlorophyll concentration for the Philippine Archipelago between 7°N and 17°N. The image is a composite of MODIS Aqua sensor images for the period of February 15–21, 2009. The area of focus for this paper, San Bernardino Strait, is outlined in white on the right center of the image. *Image courtesy of Sherwin Ladner and Robert Arnone, NRL Stennis*

(Stommel et al., 1973; Kinder and Parrilla, 1987; Bryden et al., 1994; Gomez et al., 2000; Tsimplis, 2000; Vargas et al., 2006). Research on Gibraltar has addressed a range of issues, including aspiration of deeper water (Kinder and Parrilla, 1987) and generation of internal waves and tides (Longo et al., 1992; Richez, 1994; Tsimplis, 2000; Morozov et al., 2002) as well as changes in Froude number and pressure with the compressed flow over the sill (Lafuente et al., 2000; Sannino et al., 2002).

Various studies examined a range of interactions of flow and topography in other strait regions; for example, complex three-dimensional flow structure has been observed in Knight Inlet, BC, Canada (Klymak and Gregg, 2001; Lamb, 2004). Ohlman (2011) examined surface flow along the boundaries of San Bernardino Strait simultaneous with the results discussed here, observing large vorticity and strain rates at sub-kilometer scales along the boundaries of the strait. Although maximum velocities vary widely between different straits, those observed at San Bernardino are large, with reported velocities at other sites often less than 1 m s^{-1} (e.g., Klymak and Gregg, 2001; Valle-Levinson et al., 2001; Vargas et al., 2006; Gregg and Pratt, 2010).

Few of the many studies of flow in straits and over sills throughout the world have included significant biological, optical, and/or chemical measurements. In part, difficulties associated with sampling in regions of strong flow have limited these observations. In this paper, we present observations that employ the integration of bio-optical and biogeochemical sensors into a modern tow vehicle to evaluate the variability of physical, bio-optical, and chemical signatures in the very dynamic San Bernardino Strait.

APPROACH

The challenge presented in sampling tidally dominated straits is to repeatedly occupy three-dimensional surveys rapidly enough to resolve energetic variability at tidal (in San Bernardino Strait, predominately diurnal) frequencies. To accomplish this task, we used a

Burton H. Jones *(bjones@usc.edu) is Professor (Research), Marine Environmental Biology, University of Southern California, Los Angeles, CA, USA.* **Craig M. Lee** *is Principal Oceanographer and Associate Professor, Applied Physics Laboratory, University of Washington, Seattle, WA, USA.* **Gerardo Toro-Farmer** *is PhD Candidate, University of Southern California, Los Angeles, CA, USA.* **Emmanuel S. Boss** *is Professor, University of Maine, Orono, ME, USA.* **Michael C. Gregg** *is Professor, Applied Physics Laboratory, University of Washington, Seattle, WA, USA.* **Cesar L. Villanoy** *is Professor, Marine Science Institute, University of the Philippines Diliman, Quezon City, Philippines.*

MacArtney TRIAXUS towed, undulating vehicle to map the three-dimensional distributions of physical, chemical, and inherent optical properties. TRIAXUS maintained a vertical speed of 1 m s^{-1} while typically being towed at 7 knots, with along-track horizontal resolution of 1 km or less, dependent on profile depth. TRIAXUS carried two pairs of Sea-Bird temperature and conductivity sensors along with up (1200 kHz) - and down (300 kHz)-looking RDI acoustic Doppler current profilers. Optical sensors included a WETLabs C-Star transmissometer, WETStar chlorophyll and CDOM fluorometers, WETLabs Triplet optical backscatter sensor (532, 660, and 880 nm), and a WETLabs AC-S absorption/attenuation spectrophotometer. A Sea-Bird SBE43 dissolved oxygen sensor on the vehicle measured dissolved oxygen concentration. The vehicle's sensor and engineering data were telemetered via a single-mode fiber, and recorded and displayed in real-time using the University of Washington-Applied Physics Laboratory's control and acquisition software.

The AC-S data were processed using the instrument's standard water calibration procedures performed routinely with deionized water that had been filtered through a 0.2-μ filter and UV irradiated to remove dissolved organic carbon. Temperature and salinity corrections of the attenuation and absorption data were performed according to Sullivan et al. (2006). Scattering corrections were performed based on the third method of Zaneveld et al. (1994).

In order to preserve the structure in the optical data, the full data set was processed onto a common time base of 0.25 seconds, the sampling interval of the AC-S spectrophotometer, where all times were recorded in universal time (UT). Because the absorption at 720 nm has strong temperature dependence, the 720 nm absorption was compared with the conductivity-temperature-depth (CTD) temperature data to establish the time offset between the two sensors. The AC-S data were then shifted in time to minimize the offset between the AC-S absorption at 720 nm and the CTD temperature. Once this alignment was accomplished, the other optical sensors were temporally aligned with the AC-S variables to ensure consistency of temporal and spatial alignment of all of the data.

Four optical variables derived from the absorption and attenuation measurements are used in the observations presented. Chlorophyll concentration was calculated from the AC-S absorptions at 675 and 650 nm using chlorophyll-specific absorption of 0.014 m^2 mg^{-1}) (Davis et al., 1997; Boss et al., 2007). Optical scattering, b_λ (where λ is wavelength in nm), is the difference between total attenuation (c_λ)

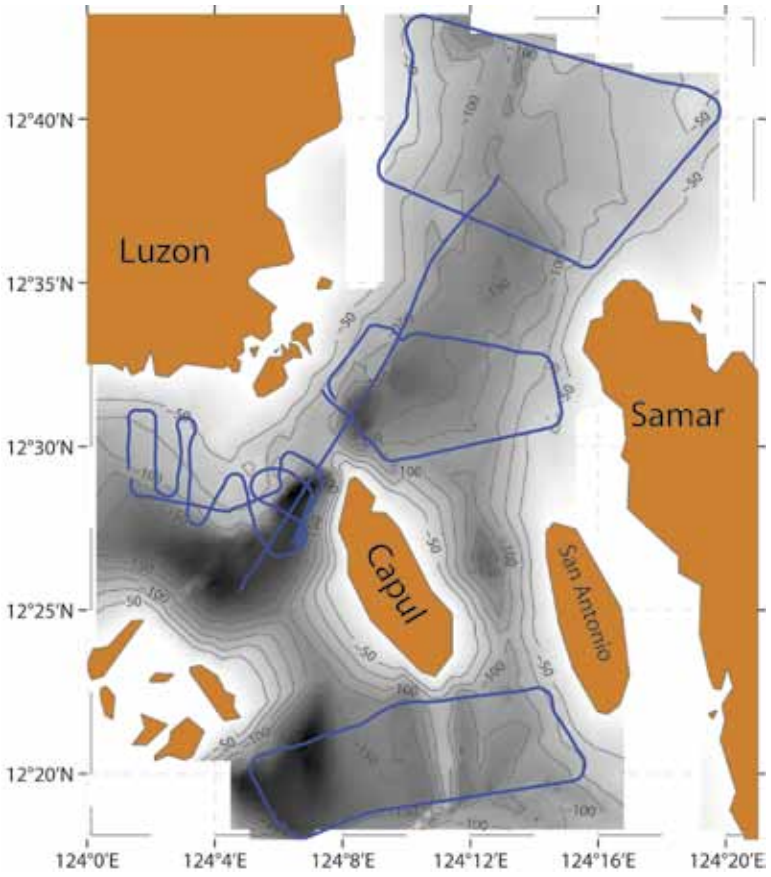

Figure 2. Topography and TRIAXUS survey tracks for the San Bernardino Strait region during February 17–21, 2009. Topography was interpolated from the ship's echosounder. Each of the survey regions, except for the most southern one, was repeatedly mapped for at least a 24-hour period. The Pacific Ocean (seaward) is north and east of the region shown; landward is toward the south and west. The San Bernardino sill is the shallow region located between the islands of Luzon and Capul.

and absorption (a_λ) (i.e., $b_\lambda = c_\lambda - a_\lambda$). Gamma ($\gamma$) is the spectral slope of $c_p(\lambda)$, the attenuation due to the particulate components in the water, fitted to a hyperbolic function (Boss et al., 2001):

$$c_p(\lambda) = c_p(\lambda_0) \cdot (\lambda/\lambda_0)^{-\gamma}.$$

Typically, $c_p(\lambda)$ is calculated by subtracting the dissolved attenuation, $c_g(\lambda)$, from the total attenuation, $c_{tot}(\lambda)$, where $c_g(\lambda)$ is essentially dissolved absorption, $a_g(\lambda)$. Because TRIAXUS did not carry a second AC-S where the inflow was filtered to provide $c_g(\lambda)$, we estimated dissolved absorption (a_g) by correlating the near-surface dissolved absorption at 400 nm, measured with an AC-S in line with the ship's near-surface flowthrough seawater system that sampled from about 5-m depth, with the vehicle's colored dissolved organic matter (CDOM) fluorescence from 4–6-m depth. The a_g spectrum was then calculated using the equation from Twardowski et al. (2004):

$$a_g(\lambda) = a_g(400) \cdot e^{-S_e(\lambda - \lambda_{400})},$$

where s_e is the spectral slope for a_g as a function of wavelength (λ). For each observation, $a_g(400)$ was estimated from the measured CDOM fluorescence, and for data from San Bernardino Strait, the value of s_e that best fit the data was 0.012. The c_p spectrum was then calculated by subtracting the estimated a_g spectrum from the measured total attenuation spectrum.

TRIAXUS surveys were planned such that multiple iterations of each survey track could be performed within a 24-hour span, thus resolving the diurnal and, often, semidiurnal tidal components within each survey pattern. To meet this rapid-sampling criteria, we planned four survey sites and a thalweg section that, when considered together, provided spatial coverage spanning critical areas of the San Bernardino Strait region (Figure 2).

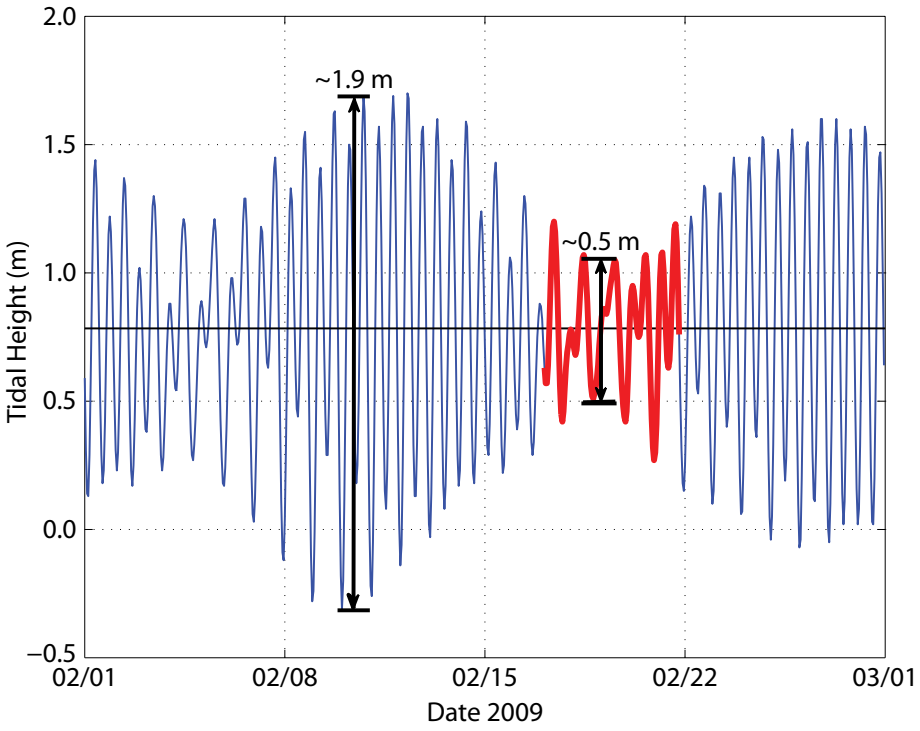

Figure 3. Measured tidal height at Legaspi, Albay, Philippines, for February 2009. The location of the tidal station is indicated in the Figure 1 inset. The red portion of the tidal series is the tidal height during the period that San Bernardino Strait was mapped for the effort described in this paper.

OBSERVATIONS

TRIAXUS surveys of San Bernardino Strait spanned the five-day period between February 17 and 21, 2009, during the neap tide (Figure 3). Diurnal variability that approximated the O1 tide (period ~ 25.8 hours; not shown) dominated during the measurement period. This timing turned out to be fortuitous because during spring tides, current velocities through the strait can reach speeds of 4–4.5 m s^{-1}, exceeding typical TRIAXUS towing speeds.

T-S Distributions within the Strait

The T-S properties for the region exhibit two major components (Figure 4): warm exterior Pacific water (above the heavy black line in Figure 4, left panel), and archipelago interior water (below the heavy black line in Figure 4). The warm Pacific water was characterized by two major end points. Exterior surface water salinity was less than 33.6 and temperature was greater than 27.5°C. Exterior deep water, in contrast, was saltier ($S > 34.4$) and found at densities (σ_θ) more than 22.75 kg m^{-3}. A third end point, exterior intermediate water, was similar in salinity to the exterior deep water, but warmer and therefore less dense. The Pacific end points were vertically layered along the outermost section. During the

period of observation (Figure 4, right panel), Pacific surface water (identified by red) entered the channel along the northwestern boundary, but did not penetrate into the interior side of the sill between Luzon and Capul (Figure 4, right panel). The intermediate water was only found in the northernmost transect. Pacific deep water penetrated across the sill into the region south of the sill at intermediate depths.

The interior water, below the heavy black line in Figure 4, was comprised of two primary components. It was characterized in the broadest sense by intermediate salinities between 34 and 34.47 and densities greater than 23 kg m^{-3}. For clarity in the graphics, a more tightly constrained characterization is used where densities are greater than 24 kg m^{-3} (Figure 4, left panel, outlined in green). The interior deep water was found below 100-m depth (Figure 4, right panel), but it also extended seaward (northeastward) of the sill during the ebb phase of the tidal cycle (not visible in Figure 4, right panel).

The interior surface water was identified as upper-layer water where chlorophyll concentrations were greater than 1 mg m^{-3} at depths less than 20 m. The brown box in Figure 4 (left panel) outlines the T-S boundaries of this shallow, high-chlorophyll water. The region with these T-S properties, though not necessarily high in chlorophyll, extended from the inner strait into the outer strait north of the sill, primarily along the eastern half of the strait (Figure 4, right panel).

Velocity Field

Figure 5 displays the three-dimensional velocity fields during both ebb and flood tides. During the ebb tide, velocities were predominantly seaward through the channel at all depths (Figure 5, left panel). Some eastward surface flow was observed north of Capul, but otherwise all flow was seaward with maximum velocities exceeding 2.5 m s^{-1} seaward of the sill north of Capul. In the outer portions of the strait, the flow along the boundaries both near Samar and in the northwest corner near Luzon was relatively slow and the direction less clear than nearer the center of the strait.

During the flood tide, although the flow was slightly more complex, most of the flow was landward into the strait (Figure 5, right panel). The maximum observed velocity was 2.3 m s^{-1} toward the southwest (landward) above the center of the sill. A weak cyclonic circulation was apparent on the west side of the tidal jet along the southern coast of Luzon. During the 24-hour period that this region was surveyed, numerous small eddies were visible in that area

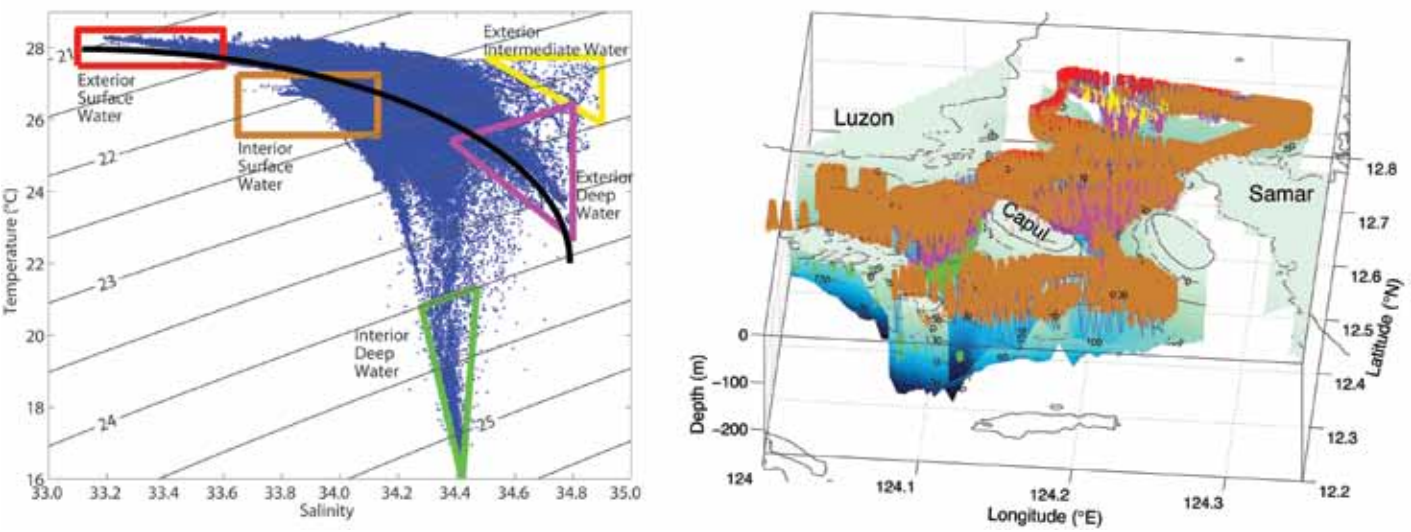

Figure 4. Water-mass distribution within the San Bernardino Strait region for the period of February 17–21, 2009. The color-coded triangles and rectangles in the left panel identify the various temperature-salinity (T-S) end points. The heavy black line in the left panel separates the exterior Pacific water above the line from the interior archipelago water below the line. The blue lines in the right panel show the vehicle path and locations for all T-S points shown in the left panel. The colors in the right panel correspond to the end points identified in the left panel (polygon colors). The regions where only blue is evident in the right panel indicate areas where the T-S values lay outside all of the end points identified in the left panel. Each survey pattern shown (see Figure 2 represents multiple passes, spanning the tidal cycle, with the TRIAXUS and its instrumentation.

along the southern coast of Luzon. Below about 140 m, in the deep basin landward of the sill, velocities were seaward (NNE) at speeds on the order of 0.1–0.2 m s^{-1}.

Overall Distribution Patterns

Distributions of salinity, chlorophyll, optical scattering at 532 nm (b_{532}), and dissolved oxygen display striking contrasts between periods of ebb and flood tides (Figure 6). During the ebb, salinity of the seaward-moving waters ranged from 33.8 to 34.4, fresher near the surface with salinity increasing with depth (Figure 6a). During ebb, interior salinities were never as high or as low as those observed in the Pacific waters that entered the strait during flood (Figure 6e). The highest chlorophyll concentrations (2–3 mg m^{-3}) occurred within the strait's interior, south of Luzon, typically within the upper 50 m. The distribution of scattering (b_{532}), indicative of suspended particle concentration, typically mirrored that of chlorophyll, with the highest particle concentrations within the strait's interior. This tight relationship between chlorophyll and backscatter did not hold in all regions. For example, a region of elevated particle concentrations but low chlorophyll was observed in the deep basin onshore of the sill (Figure 6b and c). The ebb tide carried much of the particulate matter, especially the phytoplankton, seaward into the outer portion of the strait, north of the sill. Waters with elevated chlorophyll concentrations can be seen in the northernmost line of the outer survey, perhaps moving along the eastern side of the strait. Some of the deep water with elevated particle concentrations was observed rising over the sill during the ebbing tide (Figure 6g).

The highest oxygen concentrations observed (> 220 µmol kg^{-1}) coincided with the highest chlorophyll concentrations during ebb, and were observed at the most interior portion of the strait (Figure 6d). The lowest oxygen concentrations (< 70 µmol kg^{-1}) were found in the deeper basins landward of the sill. The water carried seaward during the ebb contained intermediate oxygen concentrations, entraining water from various depths in the interior during the seaward transit. Intermediate oxygen levels (< 190 µmol kg^{-1}) in the most seaward (northern) section indicate the presence of strait interior waters, consistent with the observations of chlorophyll and b_{532}. Similar to the distribution of b_{532}, low oxygen concentrations were observed rising over the sill during ebb.

Water-column properties changed dramatically during the flood tide, as can be seen by comparing property distributions during flood (Figure 6e–h) with those from the ebb (Figure 6a–d). During flood, the strait exhibited both high and low extremes of salinity, with low salinities (< 33.5) near the surface and higher salinities (> 34.5) in the deeper layers, consistent with the T-S distribution

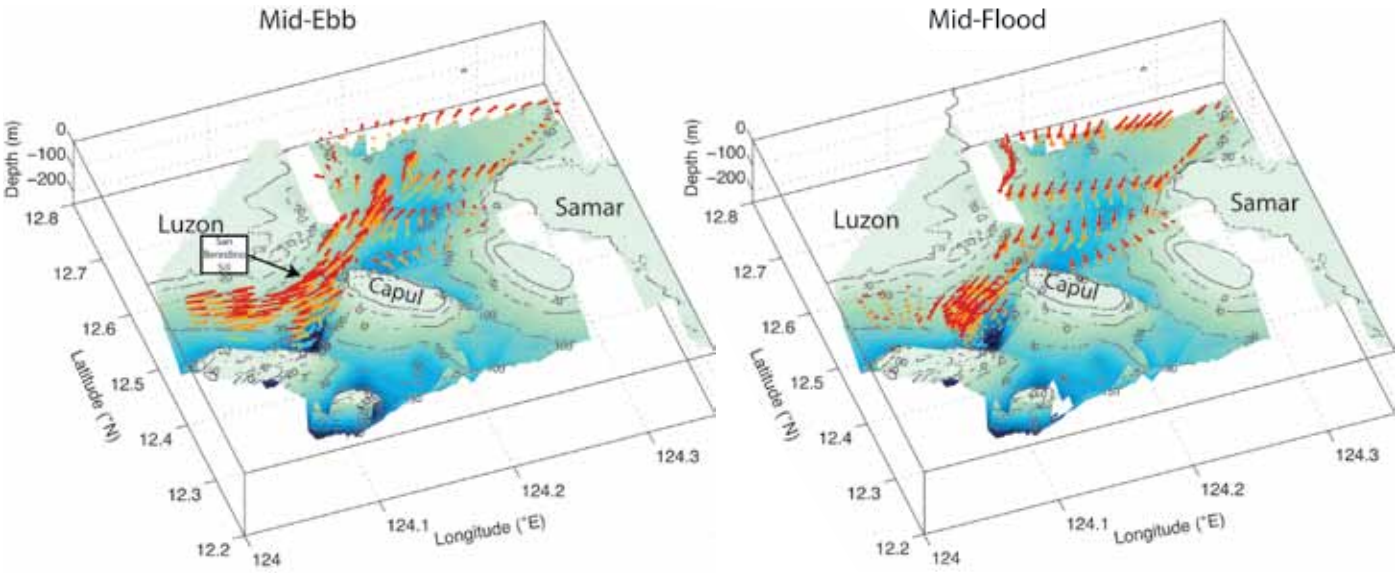

Figure 5. The three-dimensional velocity field through San Bernardino Strait during mid-ebb and mid-flood stages of the tidal cycle. The vectors are vertically averaged into 50-m bins with color from red to blue for subsequent depth layers from the surface (0–50 m) to deepest (150–200 m). The location of the San Bernardino sill is indicated in the left panel.

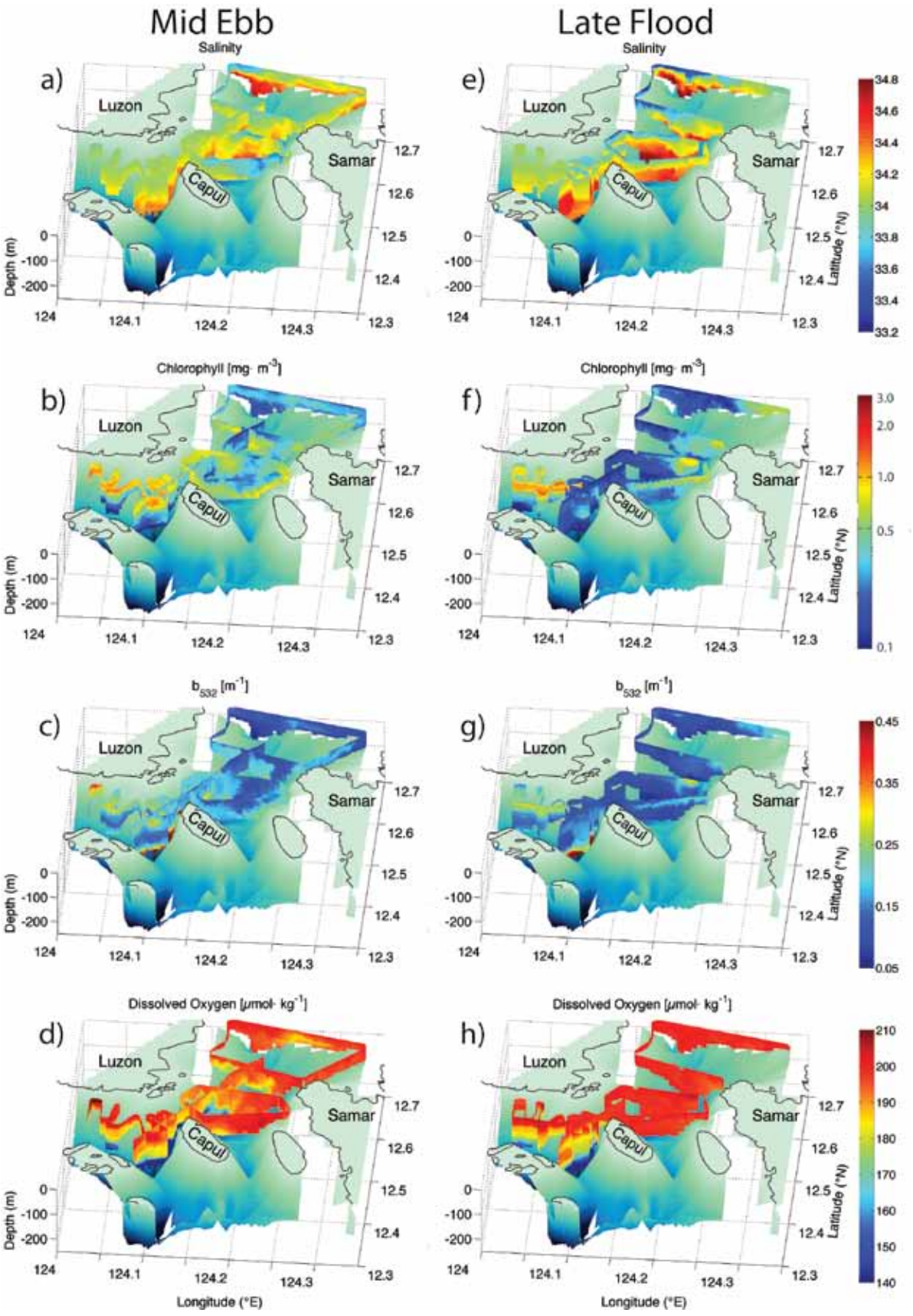

Figure 6. Three-dimensional distributions of salinity, chlorophyll, optical scattering at 532 nm (b_{532}), and dissolved oxygen during the middle ebb (left panels) and the late phase flood for the entire San Bernardino Strait region. These distributions are composites created by selecting survey passes for the same phase of the tide from the four separate surveys (Figure 2 shows the survey regions; the most southern survey region is not included).

presented earlier (Figures 4 and 6a).

Pacific waters, depleted in chlorophyll and suspended particles, penetrated across the sill and into the region south of Luzon, where a sharp frontal boundary separated them from the high-chlorophyll interior waters. Chlorophyll and b_{532} were highly correlated throughout most of the region, indicating that the particle field was phytoplankton-dominated. However, landward of the sill and adjacent to the island of Capul, low chlorophyll but high b_{532} in the upper layer indicates elevated concentration of particles other than phytoplankton.

The flood tide produced a distinctive patter in dissolved oxygen concentration. Oxygen concentrations in the incoming Pacific water exceeded 190 µmol kg^{-1} throughout the water column (Figure 6h). Oxygen concentrations landward of the sill exhibited strong vertical structure, with concentrations above 205 µmol kg^{-1} observed in the high-chlorophyll interior surface water. In the basins landward of the sill, oxygen concentration decreased with increasing density to less than 70 µmol kg^{-1} in the deepest parts of the basin. In the same region landward of the sill, west of Capul (where phytoplankton did not dominate the upper-layer particle field), oxygen concentrations less than 185 µmol kg^{-1} were observed in the upper 80 m.

Thalweg Distributions During the Late Flood Tide

An examination of the area directly over the sill provides insight into tidally driven processes. During the ebb tide, currents along the entire track were seaward throughout the water column (Figure 7a–d, black vectors). Isopycnal surfaces tended to mirror bottom topography, rising over the sill and descending again downcurrent, on the sill's seaward side (Figure 7a–d). In the upper layer, relatively high chlorophyll concentrations (0.5 to >1 mg m^{-3}), along with the associated particles (b_{532}, Figure 7c), were transported seaward across the sill. High particle loads from the lower layer were lifted over the sill but descended on the seaward side, following the isopycnals and oxygen concentration. Gamma, the spectral slope of the particulate attenuation, shows a pattern similar to that of the other variables, indicating that particles found in the lower part of the water column, landward of the sill, were larger than particles in the upper layer where σ_θ was less than 23 kg m^{-3}.

> "STRONG ARCHIPELAGO THROUGHFLOW, SUCH AS THAT OBSERVED IN THE PHILIPPINES, INTERACTS WITH COMPLEX BATHYMETRY TO PRODUCE A RANGE OF ENERGETIC FLOW REGIMES."

Toward the end of the flood, velocities were still landward in the upper layer, but weakly seaward below sill depth on the landward side of the sill. Over the sill, currents were seaward in the lower half of the water column (Figure 7e–h). This thalweg was occupied near the end of flood, and likely captured conditions as the currents were reversing. As during ebb, isopycnals rose as the flow passed over the sill, but did not sink down immediately on the lee (landward) side of the sill. Chlorophyll concentration of the incoming water was less than 0.5 mg m^{-3} along the entire section (Figure 7e). However, b_{532} in the upper 75 m increased from < ~ 0.13 m^{-1} seaward of the sill to > 0.16 m^{-1} over and landward from the sill (Figure 7g). Given the observed distribution of b_{532} (Figure 7g), the only apparent source of particulates during the flood was the deep water on the landward side of the sill.

Two additional variables, dissolved oxygen and γ, both show distributions similar to that of b_{532} during late flood. Upper-layer dissolved oxygen and γ were lower in the region where b_{532} was elevated. Like b_{532}, the only apparent source for low oxygen and low γ was the deep water landward of the sill. The optical index of refraction (η_p, not shown in the figure) exhibited the same pattern where higher values of η_p in the upper layer landward of the sill reflect the higher values below 125 m on the landward side of the sill (consistent with dominance by inorganic particles).

DISCUSSION

Vertical Flux

The patterns observed in San Bernardino Strait during the late flood tide suggest a significant vertical flux on the landward

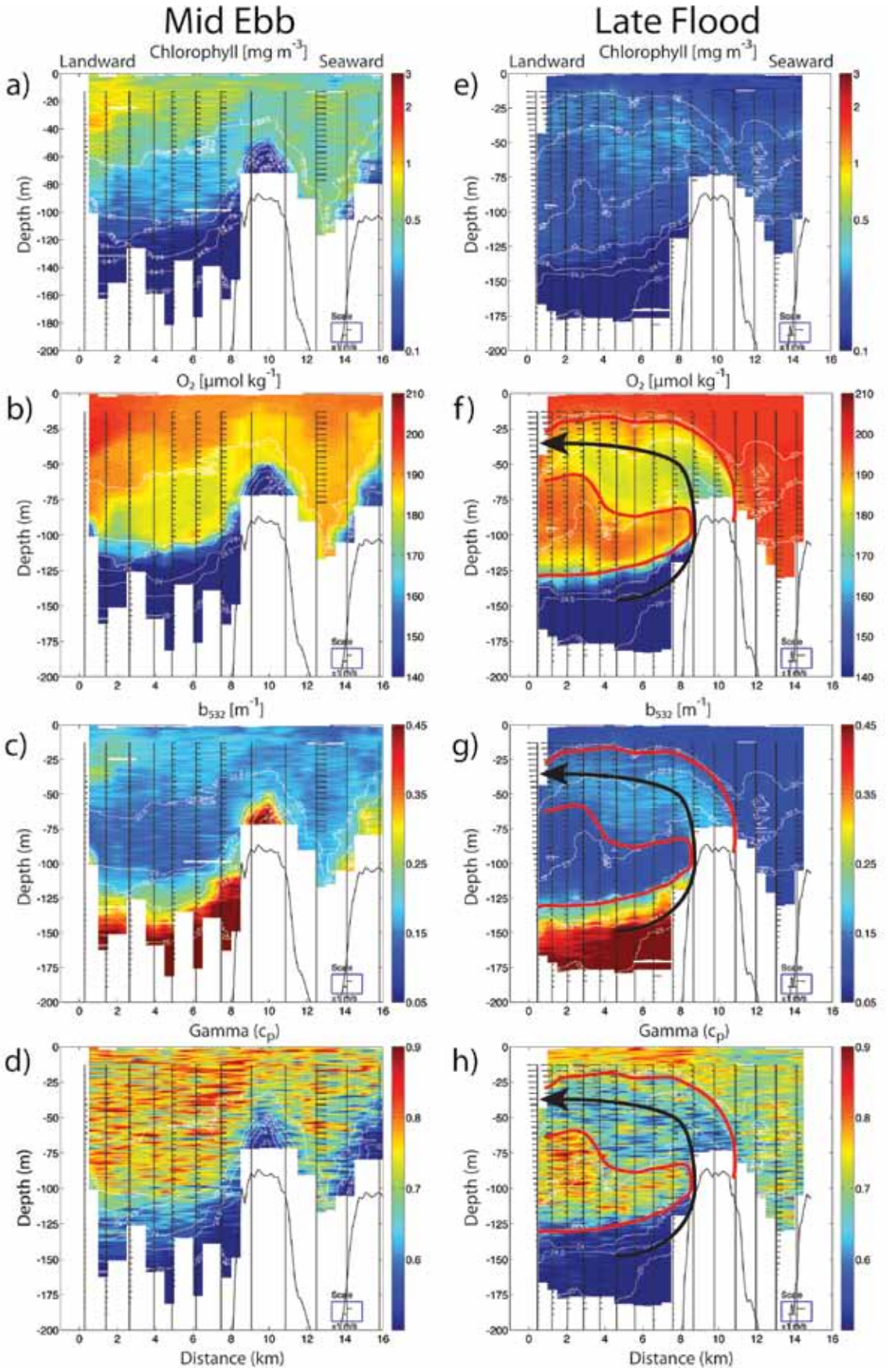

Figure 7. Sections of chlorophyll, dissolved oxygen, b_{532}, and gamma (spectral slope of c_p versus lambda) for mid-stage ebb and for late-stage flood over the San Bernardino Strait sill. Black vectors indicate the along-axis speed and direction of flow through the channel, and vertical black bars mark the centers of the averaged acoustic Doppler current profiler velocities. White contour lines indicate isopycnal surfaces. The thin black line traces bottom topography. Thick red lines outline entrained upward transport, and black curved arrows indicate transport trajectory. The lower right hand box in each panel shows the velocity vector scale of ± 1 m s^{-1}.

side of the sill during the latter half of the flood tide. This flux is supported by the distributions of chemical (dissolved oxygen) and optical (b_{532}, γ, and η_p) variables. The area of entrained water is outlined in red in the right panels of Figure 7 (panels e–h), with black arrows indicating the trajectory of water. When the end points of these distributions are plotted on a T-S diagram, they indicate that vertical transport and mixing on the landward side of the sill during the flood tide results in diapycnal mixing and entrainment into the upper layer (Figure 8). Deep water from the basin on the landward side of the sill (black circles in Figure 8) is vertically advected into the upper layer at the top of the sill (red circles between densities of 22.5 and 23.2, Figure 8). From the top of the sill, the aspirated water is transported landward and vertically, mixing into the upper 15–80 m of the water column landward from the sill. Additional mixing between exterior low-salinity water and interior basin water upwelled at the sill produces the waters where elevated chlorophyll concentrations were observed (yellow dots in Figure 8).

At the time scale of these observations (hours), oxygen can be considered to be a conservative tracer. The median concentration of dissolved oxygen in the deep water ($\sigma_\theta > 24.5$ landward of the sill) was 79.3 μmol kg^{-1} and in the landward flowing upper layer (depth < 75 m seaward of the sill), the median concentration was 197 μmol kg^{-1}. Using these two concentrations as endpoints, the final mixture in the entrained subsurface water landward of the sill contained 13.4% deep water.

Temperature, salinity, oxygen, and nitrate data from the World Ocean Data Base (WODB; Boyer et al., 2006) were used to construct a nitrate section for the late flood thalweg section. The WODB T-S data available for the strait were consistent with the T-S distribution obtained from the cruise. Low oxygen concentrations in the deeper landward basin suggest that organic matter has been remineralized through microbial nutrient cycling. Nitrate and oxygen exhibited a negative correlation where

$$[NO_3\ (\mu mol\ l^{-1})] = -0.156 \cdot [O_2\ (\mu mol\ kg^{-1})] + 33.5.$$

Because the mixing time from the deep basin into the upper layer was at most a few hours, both oxygen and nitrate are assumed to be conservative over this short time period. The resulting nitrate section indicates concentrations of 5–7 μmol l^{-1} in the upper layer after vertical transport and mixing of the deeper water into the upper, exterior Pacific water layer (Figure 9). These nitrate concentrations are consistent with the chlorophyll concentrations observed within the interior of the strait.

Observed distributions of chemical and optical variables indicate significant vertical entrainment and diapycnal mixing during the latter half of the flood tide. This flux appears linked to accelerated flow over the sill. During the mid-flood observations, although the flow

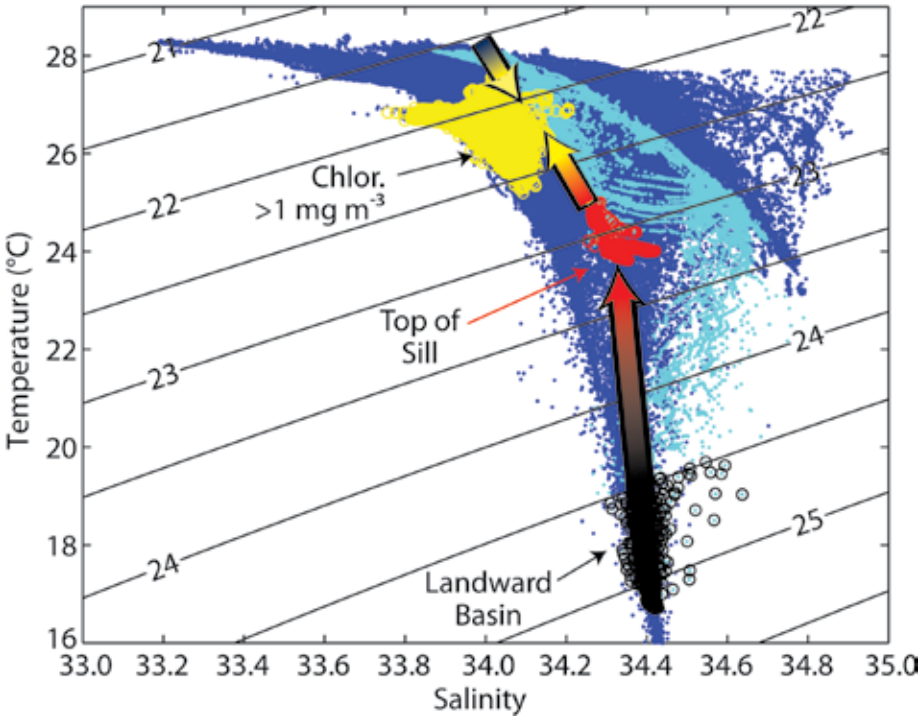

Figure 8. Temperature-salinity (T-S) diagram indicating the pathway of deep water from the landward side of the sill into the upper layer. Darker blue data points correspond to all of the data from the region (Figure 4). Light blue points are the data from the late-flood thalweg transect over the sill. After entrainment of the deeper water from the landward basin (black circles) into the upper layer (red circles indicate T-S at the top of the sill; black-red arrow), horizontal mixing between the entrained deep water and interior upper layer water (red-yellow and blue-yellow arrows) leads to development of a phytoplankton bloom (yellow dots) in the interior part of San Bernardino Strait.

is at critical speeds (Fr ≥ 1) along the entire transect, the Froude number rises to ~ 2 immediately landward of the sill (~ 8 km), due to a deepened mixed layer and decreased local stratification.

These observations were obtained during the neap phase of the neap-spring tidal cycle (Figure 3). Tidal velocities in the region have been observed up to 4.5 m s^{-1} (Peña and Mariño, 2009). It is expected that during spring tide, vertical transport and mixing processes will be significantly stronger. Velocities over the sill may be nearly twice the values that we observed. Froude numbers would increase significantly, and the pressure drop due to acceleration of currents over the sill would also increase. As a result, it is likely that the mixing pathways shown in Figure 8 will be shifted toward the left in T-S space, corresponding to the observations along the left edge of the T-S distribution. Therefore, the flux of nitrate is on the low end of the concentrations, and the mixing and transport into the interior will extend farther into the strait than was observed during February 17–21, 2009.

Aspiration, within the context of flow over sills, is the process where deeper water is transported upward from below the sill depth and entrained into flow above the sill. It has been observed at other sills and was suggested by one of the earliest evaluations of sill flow from Gibraltar Strait (Stommel et al., 1973). Aspiration of deep water from the upcurrent side of the sill has been described theoretically (Lane-Serff, 2004) and demonstrated observationally (Kinder and Parrilla, 1987; Seim and Gregg, 1997). The aspiration of deeper water in San Bernardino Strait is evident during mid-flood when water from the upcurrent side of the sill rises from more than 150-m depth to the sill top at 90 m, where it becomes entrained into the landward flow of the upper layer. During mid-flood, flow at 140 m is 0.1–0.2 m s^{-1} seaward, opposite in direction to the tidally driven upper layer flow over the sill. It may be that this flow strengthens as the upper layer flow weakens during late flood, and the reduced pressure of ~ 1000 Pa (based on a simple Bernoulli calculation) over the sill relative to the upcurrent region facilitates vertical transport into the upper layer and mixing with the water entering the strait from the Pacific side. To our knowledge, the observed aspiration of deeper water from the lee side of the sill has not been reported previously.

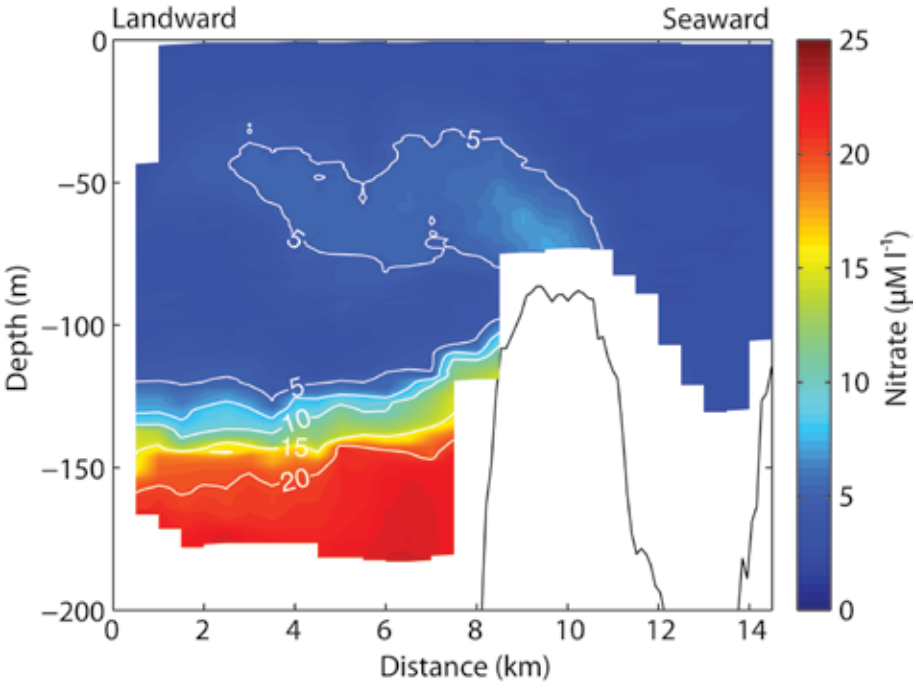

Figure 9. An estimate of the distribution of nitrate based on oxygen concentration for the late flood thalweg across the San Bernardino Strait sill (8–12 km). Both color and white contour lines indicate nitrate concentration.

Horizontal Flux

The observations show biomass accumulation within the strait and seaward advection into the outer strait during the ebb (Figures 6 and 7). To evaluate whether there is a net flux of biomass through the strait, we examined the flux across the seaward side of the sill using the portion of survey region 2 that is closest to and parallel with the sill (Figure 2). Flux was calculated by combining the chlorophyll concentration ($Chl_{x,z,t}$) and the along-axis velocity ($V_{x,z,t}$) over the course of a tidal cycle:

$$Net\_transport = \sum_{t=0}^{t_{tide}} \sum_{x=0}^{x_{max}} \sum_{z=0}^{z_{max}} Chl(x,z,t) \cdot \vec{V}(x,z,t) \cdot \Delta t.$$

Flux was calculated over a section that was 3.5-km wide and spanned the deep (bottom depth greater than 100 m) portion of the channel. The calculation

was restricted to the upper 100 m of the water column because that is where the bulk of the phytoplankton chlorophyll was observed. The net flux for approximately one tidal cycle (~ 24 hours) is ~ 4000 kg Chl into the strait.

Other Processes

Other processes in the interior are likely to contribute to nutrient fluxes and phytoplankton production of the high-chlorophyll region within the strait. A broad region of high chlorophyll west of Capul suggests that tidally driven mixing may also be contributing the nutrient flux, leading to the high chlorophyll of this region (Sharples et al., 2001; Macias et al., 2007). Although the interior was studied with less detail than the region near Capul and the area north of the sill, tidal mixing may also contribute a significant vertical flux of deep water during the late flood.

> "SUBSURFACE TOPOGRAPHY, AT LEAST AS COMPLEX AS THE TERRESTRIAL TOPOGRAPHY, INCLUDES MANY BETWEEN-ISLAND STRAITS AND SILLS WITH COMPLEX SHAPES."

Chlorophyll concentrations were higher seaward of the strait during ebb and low in this region during flood. This difference in chlorophyll concentrations between the ebb (higher chlorophyll) and flood (lower chlorophyll) suggests that the net flux of chlorophyll could be seaward, provided that the volume flux is symmetric between the ebb and flood tidal phases. However, for the 28-hour period spent occupying survey 2, the flow was landward for 17.4 hours. Net chlorophyll flux through the strait is consistent with the net landward flow through the strait between Capul and Luzon. Whether this net landward transport is sustained over a complete spring-neap cycle is unknown. One result of this unbalanced flow, if it is sustained, is that it may lengthen the retention time of nutrients that are transported into the upper layer, and thus allow for the integration and accumulation of the nutrients into the observed biomass.

CONCLUSIONS

Observations from the sill of San Bernardino Strait are distinct from previously reported flows over sills in at least two respects. The maximum speed of flows over the San Bernardino Strait sill exceeds 2.5 m s^{-1}, significantly greater than the flows observed at Hood Canal (0.5–0.6 m s^{-1}; Gregg and Pratt, 2010); at Knight Inlet, British Columbia (Klymak and Gregg, 2001); or in a Chilean fjord, O(1 m s^{-1}) (Valle-Levinson et al., 2001). These velocities are expected to nearly double during the spring phase of the spring-neap cycle. The combination of physical, optical, and chemical measurements collected by the heavily instrumented TRIAXUS towed profiler captured aspiration of deep water from the landward side of the sill during flood tide. This aspiration mixes deep waters into the upper layer and, through injection of nutrients into the upper layer, likely contributes to elevated phytoplankton productivity and the associated biomass increase landward of the sill. During the measurement period, there were net fluxes of mass and chlorophyll within the upper 100 m into the strait through the channel between Luzon and Capul.

ACKNOWLEDGEMENTS

We thank the captain and crew of R/V *Melville* for their able support during the cruise. The efforts of Jason Gobat, Eric Boget, Adam Huxtable, Matthew Ragan, and Joe Martin were essential to the success of this effort. Sherwin Ladner, Richard Gould, and Robert Arnone of the Naval Research Laboratory at Stennis, MS, generously provided remote-sensing imagery. Joe Martin provided the reprocessed ADCP data from the cruise. Bridget Seegers contributed helpful comments on the manuscript. Legaspi tide gauge data were provided by NAMRIA, Philippines. This effort was supported by the Office of Naval Research (Award nos. N00014-06-1-0688 for Jones, N00014-06-1-0916 for Boss, N00014-06-1-0687 for Lee and Gregg, and N00014-06-1-0686 to Cesar Villanoy through Pierre Flament, University of Hawaii).

REFERENCES

Boss, E., W.S. Pegau, W.D. Gardner, J.R.V. Zaneveld, A.H. Barnard, M.S. Twardowski, G.C. Chang, and T.D. Dickey. 2001. Spectral particulate attenuation and particle size distribution in the bottom boundary layer of a continental shelf. *Journal of Geophysical Research* 106(C5):9,509–9,516.

Boss, E.S., R. Collier, G. Larson, K. Fennel, and W.S. Pegau. 2007. Measurements of spectral optical properties and their relation to biogeochemical variables and processes in Crater Lake, Crater Lake National Park, OR. *Hydrobiologia* 574:149–159, doi:10.1007/S10750-006-2609-3.

Boyer, T.P., J.I. Antonov, H.E. Garcia, D.R. Johnson, R.A. Locarnini, A.V. Mishonov, M.T. Pitcher, O.K. Baranova, and I.V. Smolyar. 2006. *World Ocean Database 2005*. S. Levitus, ed., NOAA Atlas NESDIS 60, US Government Printing Office, Washington, DC, 190 pp., DVDs.

Bryden, H.L., J. Candela, and T.H. Kinder. 1994. Exchange through the Strait of Gibraltar. *Progress in Oceanography* 33(3):201–248.

Davis, R.F., C.C. Moore, J.R.V. Zaneveld, and J.M. Napp. 1997. Reducing the effects of fouling on chlorophyll estimates derived from long-term deployments of optical instruments. *Journal of Geophysical Research* 102:5,851–5,855.

Gomez, F., N. Gonzalez, F. Echevarria, and C.M. Garcia. 2000. Distribution and fluxes of dissolved nutrients in the Strait of Gibraltar and its relationships to microphytoplankton biomass. *Estuarine Coastal and Shelf Science* 51(4):439-449, doi:10.1006/Ecss.2000.0689.

Gordon, A.L., J. Sprintall, and A. Ffield. 2011. Regional oceanography of the Philippine Archipelago. *Oceanography* 24(1):14–27.

Gregg, M.C., and L.J. Pratt. 2010. Flow and hydraulics near the sill of Hood Canal, a strongly sheared, continuously stratified fjord. *Journal of Physical Oceanography* 40(5):1,087–1,105, doi:10.1175/2010jpo4312.1.

Jones, A.T., and W. Rowley. 2002. Global perspective: Economic forecast for renewable ocean energy technologies. *IEEE Marine Technology Society Journal* 36(4):85–90, doi:10.4031/002533202787908608.

Kinder, T.H., and G. Parrilla. 1987. Yes, some of the Mediterranean outflow does come from great depth. *Journal of Geophysical Research* 92(C3):2,901–2,906.

Klymak, J.M., and M.C. Gregg. 2001. Three-dimensional nature of flow near a sill. *Journal of Geophysical Research* 106(C10):22,295–22,311.

Lafuente, J.G., J.M. Vargas, F. Plaza, T. Sarhan, J. Candela, and B. Bascheck. 2000. Tide at the eastern section of the Strait of Gibraltar. *Journal of Geophysical Research* 105(C6):14,197–14,213.

Lamb, K.G. 2004. On boundary-layer separation and internal wave generation at the Knight Inlet sill. *Proceedings of the Royal Society of London Series A* 460(2048):2,305–2,337.

Lane-Serff, G.F. 2004. Topographic and boundary effects on steady and unsteady flow through straits. *Deep-Sea Research Part II* 51(4–5):321–334, doi:10.1016/J.Dsr2.2003.07.019.

Longo, A., M. Manzo, and S. Pierini. 1992. A model for the generation of nonlinear internal tides in the Strait of Gibraltar. *Oceanologica Acta* 15(3):233–243.

Macias, D., A.P. Martin, J. Garcia-Lafuente, C.M. Garcia, A. Yool, M. Bruno, A. Vazquez-Escobar, A. Izquierdo, D.V. Sein, and F. Echevarria. 2007. Analysis of mixing and biogeochemical tides on the Atlantic-Mediterranean effects induced by flow in the Strait of Gibraltar through a physical-biological coupled model. *Progress in Oceanography* 74(2–3):252–272, doi:10.1016/J.Poccan.2007.04.006.

Morozov, E.G., K. Trulsen, M.G. Velarde, and V.I. Vlasenko. 2002. Internal tides in the Strait of Gibraltar. *Journal of Physical Oceanography* 32(11):3,193–3,206.

Ohlmann, J.C. 2011. Drifter observations of small-scale flows in the Philippine Archipelago. *Oceanography* 24(1):122–129.

Peña, N.A., and A.G. Mariño. 2009. Marine current energy initiatives in the Philippines. Paper presented at the East Asian Seas Congress 2009, Manila, Philippines. Powerpoint slides available at: http://pemsea.org/eascongress/international-conference/presentation_t4-1_pena.pdf (accessed January 15, 2011).

Pullen, J., J.D. Doyle, P. May, C. Chavanne, P. Flament, and R.A. Arnone. 2008. Monsoon surges trigger oceanic eddy formation and propagation in the lee of the Philippine Islands. *Geophysical Research Letters* 35(7), L07604, doi:10.1029/2007gl033109.

Richez, C. 1994. Airborne synthetic-aperture radar tracking of internal waves in the Strait of Gibraltar. *Progress in Oceanography* 33(2):93–97.

Sannino, G., A. Bargagli, and V. Artale. 2002. Numerical modeling of the mean exchange through the Strait of Gibraltar. *Journal of Geophysical Research* 107(C8), 3094, doi:10.1029/2001jc000929.

Seim, H.E., and M.C. Gregg. 1997. The importance of aspiration and channel curvature in producing strong vertical mixing over a sill. *Journal of Geophysical Research* 102(C2):3,451–3,472.

Sharples, J., C.M. Moore, T.P. Rippeth, P.M. Holligan, D.J. Hydes, N.R. Fisher, and J.H. Simpson. 2001. Phytoplankton distribution and survival in the thermocline. *Limnology and Oceanography* 46(3):486–496.

Stommel, H., H. Bryden, and P. Mangelsdorf. 1973. Does some of the Mediterranean outflow come from great depth? *Pure and Applied Geophysics* 105:879–889.

Sullivan, J.M., M.S. Twardowski, J.R.V. Zaneveld, C.M. Moore, A.H. Barnard, P.L. Donaghay, and B. Rhoades. 2006. Hyperspectral temperature and salt dependencies of absorption by water and heavy water in the 400–750 nm spectral range. *Applied Optics* 45(21):5,294–5,309, doi:10.1364/AO.45.005294.

Tsimplis, M.N. 2000. Vertical structure of tidal currents over the camarinal sill at the Strait of Gibraltar. *Journal of Geophysical Research* 105(C8):19,709–19,728.

Twardowski, M.S., E. Boss, J.M. Sullivan, and P.L. Donaghay. 2004. Modeling the spectral shape of absorption by chromophoric dissolved organic matter. *Marine Chemistry* 89(1–4):69–88.

Valle-Levinson, A., F. Jara, C. Molinet, and D. Soto. 2001. Observations of intratidal variability of flows over a sill/contraction combination in a Chilean fjord. *Journal of Geophysical Research* 106(C4):7,051–7,064.

Vargas, J.M., J. Garcia-Lafuente, J. Candela, and A.J. Sanchez. 2006. Fortnightly and monthly variability of the exchange through the Strait of Gibraltar. *Progress in Oceanography* 70(2–4):466–485, doi:10.1016/J.Pocean.2006.07.001.

Zaneveld, R.V., J.C. Kitchen, and C. Moore. 1994. The scattering error correction of reflecting-tube absorption meters. *Ocean Optics XII* 2258:44–55, doi:10.1117/12.190095.